ADAPTIVE ACQUISITION TECHNIQUES FOR PLANAR NEAR-FIELD ANTENNA MEASUREMENTS – PART 2

Daniël Janse van Rensburg
Nearfield Systems Inc.
19730 Magellan Drive,
Torrance, CA 90502-1104, USA

ABSTRACT

The use of adaptive acquisition techniques to reduce the overall test time in planar near-field antenna measurements was presented in [1] & [2]. In those publications the concept of a decision function to track the uncertainty of a measurement as the data acquisition proceeds and also to adapt the acquisition region dynamically, was introduced. In this publication we build upon that work and present the concept of near-field array initialization. This is tested on different antennas and simulation results are presented. We also present actual measurement results to validate simulations that have to date been used to demonstrate advantages of the adaptive techniques.

Keywords: Antenna measurements, planar near-field, adaptive.

1 Introduction

Planar near-field antenna testing usually involves sampling of a rectangular area that is simply acquired from one end to the other by linear motion of the near-field probe. This can be achieved by continuous probe motion in the one direction and step-wise motion in the orthogonal direction. This method is well understood and widely used. However, this approach is very limiting in that none of the data acquired is being used during the acquisition process to guide or ultimately terminate the acquisition. The techniques presented in [1] & [2] attempted to exploit this information in order to reduce test times and intelligently guide these acquisitions.

When planar near-field data sets are inspected, it is obvious that significant test time can be spent measuring very low signal levels that may be of limited value to the final far-field result. Also, the order of acquisition is such that a final test result is only achieved at the end of the acquisition, whereas an adaptive technique allows for sampling of the regions of significant energy first, displaying the far-field result immediately and then refining this result as testing progresses. This approach provides the user with a fairly reliable test result early in the acquisition process and therefore allows for immediate assessment of the data, test time savings and the option of early termination, if appropriate.

The adaptive acquisition technique also allows for directed attention at far-field parameters of interest and using those to guide the acquisition process. Determination of a parameter like AUT gain or directivity, for instance, can lead to significant test time reduction in contrast to a low level side lobe that may require the acquisition of a larger data set.

In this paper test data for two acquisition schemes (rectangular spiral & adaptive rectangular loop) are presented and compared to the traditional acquisition process. Both acquisition schemes rely on the processing of the measured data during the acquisition process to assess far-field parameters and determine a suitable point of termination. The second adaptive technique also steers the near-field acquisition based on sampled data and is therefore a truly adaptive process. Potential test time reductions using these techniques are presented and actual test data obtained from a hardware implementation is shown. The two acquisition schemes and decision functions are reviewed in Section 2. In Section 3 the concept of near-field array initialization is presented as a method for accelerating acquisition convergence. A selection of test cases is presented in Section 4 and these results demonstrate the advantages and limitations of the acquisition schemes by comparing results to that obtained using the traditional acquisition process. Test times based on actual measurement to confirm simulation results are presented in Section 5.

2 Planar Near-field Acquisition Techniques

In planar near-field [PNF] testing the near-field scan region is principally sized based upon the AUT aperture size, the aperture to near-field probe separation distance and the maximum far-field angles of interest. This translates into a widely used approximate rule (which has been established experimentally and derived theoretically) that is given in [3] as $L \geq W + P + 2H \tan\xi$ where angle ξ is measured from broadside, L is the distance of the PNF probe traverse, H is the separation between the AUT and probe, P is the probe aperture dimension, and W is the AUT aperture dimension. This rule therefore gives us the minimum L required for a given angular region of validity and is depicted in Figure 1.

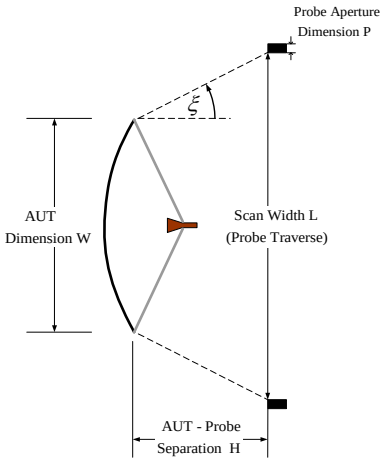

Figure 1 - Sketch showing the AUT aperture size and scan region dimensions.

For PNF acquisition a rectangular region of measurement of width *x* and height *y* is defined by applying this rule in the two orthogonal planes of interest. Data samples are acquired in *λ/2* intervals throughout this region. The sequence of acquisition of these data samples is as depicted in Figure 2 and will be referred to as the "traditional method" below. This method of acquisition requires mechanical and RF acquisition time and upon completion the desired far-field data can be evaluated.

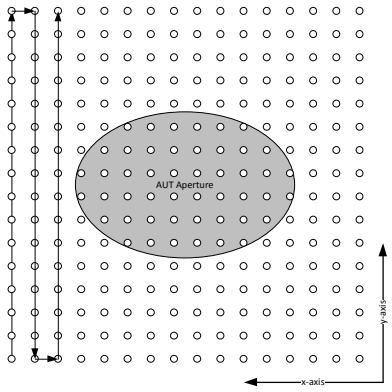

Figure 2 – A traditional rectangular PNF acquisition. Near-field grid points (o) are shown superimposed on the AUT aperture (shaded). Data is acquired by motion of the probe in the y-direction while stepping in the x-direction after completion of each y-cut.

The first of the new acquisition techniques proposed in [1] is depicted in Figure 3. The probe moves on a rectangular spiral locus (as indicated), encompassing an increasingly larger number of sampling points as it moves. Acquisition starts at the center of the AUT aperture and progresses outward. Each spiral ring is regarded as an iteration in this instance and if we have a collection of sampled near-field values at the $(n-1)^{th}$ stage, as indicated by the locus (red) in Figure 3, we then let the probe continue along its data acquisition path until at the n^{th} stage we have an additional number of data points, as indicated by the locus (green) in Figure 3. Since the far-zone field computation time is very small compared to the data acquisition time and can be done repeatedly while the data is being acquired, we use the far-field information through decision functions to impact near-field acquisition termination after the n^{th} stage.

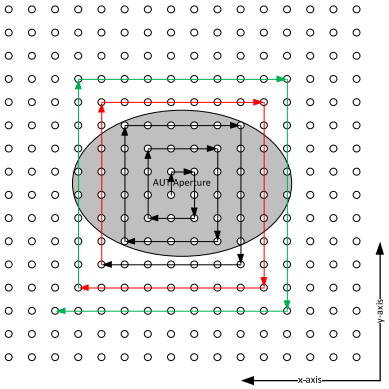

Figure 3 – Rectangular spiral PNF acquisition. Near-field grid points (o) are shown superimposed on the AUT aperture (shaded) and probe path history after $(n-1)^{th}$ (red) and n^{th} (green) iterations.

The second of the two acquisition techniques proposed in [1] is depicted in Figure 4. The probe moves on a rectangular loop locus (as indicated), encompassing an increasingly larger number of sampling points as it moves away from the center of the AUT aperture. Each rectangular data ring is regarded as an iteration in this instance. At the end of the $(n-1)^{th}$ iteration the measured near-field power on each of the four sides of the loop are evaluated and the region of acquisition is expanded in the direction of the maximum power level by adding two rows or columns of data (dashed locus in Figure 4). After this additional acquisition the n^{th} iteration consists of a full rectangular data loop again and the process is repeated. The advantage of this acquisition is twofold. Firstly, the region of acquisition grows in the direction of higher near-field energy. This makes the method ideally suited for AUT aperture distributions that are elliptical or even asymmetric. Secondly, the method ensures that valid near-field data is being acquired during all scanner motion, thereby maximizing efficiency of the mechanical process.

For both of these methods, decisions functions are required to assess convergence of the desired far-field data. These decision functions are evaluated at the end of each iteration. In [1] we defined relevant decision functions and they are presented here in cursory form for completeness.

Our first decision function is based on the co-polarized partial directivity in direction (θ,ϕ) and can be computed from the plane wave spectrum using

$$D_{co}(\theta,\phi) = 4\pi\left|E_{co}(\theta,\phi)\right|^2 \Big/ 2\eta_o P_{rad}$$

where η_o is the free space intrinsic impedance and the total radiated power P_{rad} is found from the plane wave spectrum [3, p. 115]. We observe the directivity in the direction of maximum radiation as the scan size increases. At some point the directivity value changes negligibly from the n^{th} to the $(n\text{-}1)^{th}$ iteration. If this change is less than a certain amount, say the known accuracy within which the directivity can be determined by the measurement set-up, this can be used to terminate the PNF acquisition.

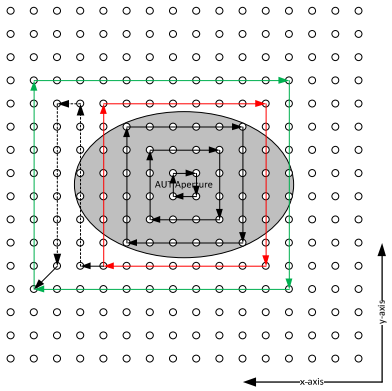

Figure 4 – Adaptive rectangular loop PNF acquisition scheme. Near-field grid points (o) are shown superimposed on the AUT aperture (shaded) and probe path history after (n-1)th (red) and nth (green) iterations.

Our second decision function is based on the normalized pattern differences between scan iterations. After the n^{th} and $(n\text{-}1)^{th}$ scan iterations we denote the far-zone co-polarized electric field value in direction (θ_i,ϕ_j) by $E_{co}^{n}\left(\theta_i,\phi_j\right)$ and $E_{co}^{n-1}\left(\theta_i,\phi_j\right)$, respectively. The error term in direction (θ_i,ϕ_j) is, after the n^{th} iteration, then

$$f_{co}^{n}\left(\theta_i,\phi_j\right) = \frac{\left|E_{co}^{n}\left(\theta_i,\phi_j\right)\right| - \left|E_{co}^{n-1}\left(\theta_i,\phi_j\right)\right|}{\max\limits_{i,j}\left\{\left|E_{co}^{n}\left(\theta_i,\phi_j\right)\right|\right\}}$$

In other words, the error measure in each pattern direction is the difference between the normalized n^{th} and $(n\text{-}1)^{th}$ patterns in that direction. In all decision function work the full three-dimensional pattern is considered rather than just single pattern cuts. The normalization factor is simply the maximum field magnitude after the n^{th} iteration. This error term is direction dependent and in the results presented here we select for each test case the direction of a specific side lobe of interest. Therefore, if the normalized radiation pattern magnitude in direction (θ_i,ϕ_j) is E_{dB}, and we wish the uncertainty there to be $\pm\Delta_{dB}$, then we require

$$20\log\left|f_{co}^{n}\left(\theta_i,\phi_j\right)\right| \le E_{dB} + 20\log\left\{1-10^{-\Delta_{dB}/20}\right\}$$

3 Near-field Array Initialization

The results presented in [1] outlined the efficiency of the acquisition techniques described in Section 2 and the potential test time reductions. However, these results also exposed the sensitivity of these techniques to severe truncation effects, especially during the initial phases of the acquisition (during measurement of regions of high energy). This observation lead to the investigation of initializing the near-field arrays with data measured along the center lines of the PNF scan region (say N_x points along the x-axis and N_y points along the y-axis). The intent of this action would be to conduct an initial exploratory acquisition along these two lines and to use this information to populate the entire near-field data array with interpolated data using the N_x x N_y data points. Data is then still acquired using the techniques described before, but the impact of truncation is "softened" since data is now being refined during the acquisition process instead of "adjusted" from zero. If the normalized data measured along the x and y-axes are denoted as $F_n(x,0)$ and $F_n(0,y)$ respectively (where normalization is w.r.t. $F(0,0)$ at the intersection point), then the full near-field data array is initialized using the following interpolation rule

$$F(x,y) = F_n(x,0).F_n(0,y).F(0,0)$$

This process can be demonstrated by the results presented below in Figure 5 where a full data set in shown first, the two orthogonal measured data cuts $F_n(x,0)$ and $F_n(0,y)$ are shown second and the interpolated data set is shown as the third image. By comparing the first and third images, the method appears to be working fairly well and this is confirmed once the corresponding far-field pattern cuts are extracted as shown in Figure 6. This comparison shows that pattern agreement can be obtained to within a -35 dB error level by only using 2% of the full data set. This advantage is therefore gained at the cost of a pre-measurement of two near-field cuts, This typically represent a 2% - 3% increase in test time for most near-field data sets. It should also be realized that the method works particularly well for rectangular aperture type antennas with separable distributions and less so for apertures that do not conform to this norm. Also, pattern fidelity in the principal planes seems to be much higher than for the inter-cardinal planes. Nevertheless, it is found that this initialization of the near-field arrays aids convergence for all the test cases considered here, regardless of aperture type.

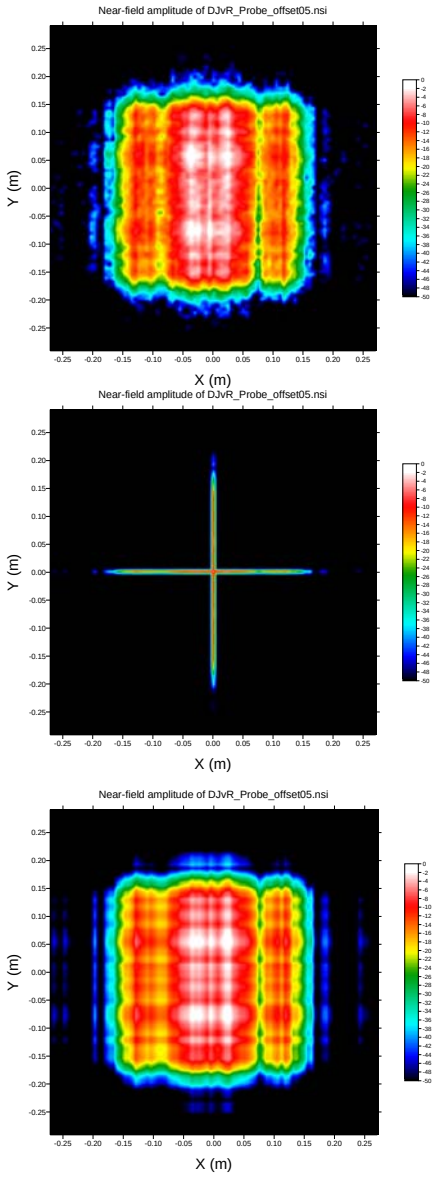

Figure 5 – The first image shows a near-field amplitude distribution. The second image shows two linear cuts measured along the orthogonal center lines of the scan region. The third image shows the interpolated near-field array based on these center cuts only.

4.0 Test Case Studies

The acquisition techniques outlined in Section 2 and the array initialization described in Section 3, were tested on four distinct antenna test cases. In all of these cases PNF data sets were acquired as reference baselines. The adaptive acquisition techniques were then applied in simulation and potential test time reductions estimated. The decision functions described in Section 2 were used and applied to the AUT directivity and a specific side lobe in each instance. The specific AUT's considered are as shown in Table 1.

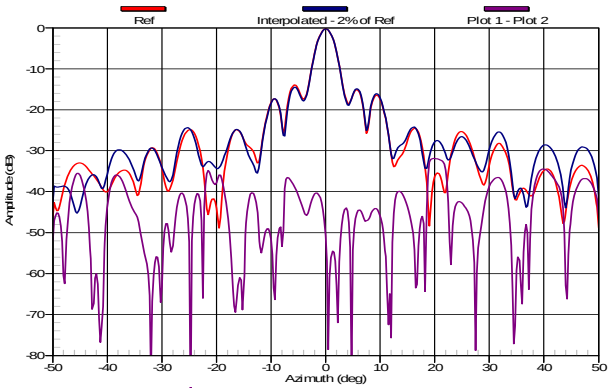

Figure 6 – Far-field principal plane cut extracted from the near-field amplitude distribution shown in Figure 5 versus far-field principal plane cut extracted from the interpolated near-field amplitude distribution shown in Figure 5.

Table 1 – Summary of AUT test cases considered.

AUT#	Antenna Type	Operating Frequency [GHz]	Maximum Directivity [dBi]
1	Dual offset reflector	14.5 GHz	39
2	Slotted waveguide array	23 GHz	37
3	Offset reflector	12 GHz	31
4	Monopulse antenna	10.5 GHz	N/A

Figure 7 shows the progression of AUT directivity for AUT #1 as a function of relative acquisition time (expressed as a % of the full data set as acquired using a traditional method) for the three methods. The blue curve represents the traditional acquisition case and clearly shows little convergence during the initial acquisition phase. Final convergence is achieved at roughly 75% of the full data set. The red curve shows the rectangular spiral case and the rapid convergence is clear with stable solution achieved at about 20% of the traditional data set. The green curve shows the adaptive rectangular case with the array initialization as described in Section 3, applied. It is clear that this process provides an excellent starting point for the acquisition and that a stable directivity solution is achieved at about 15% of the traditional data set, while even the value obtained after 3% is quite acceptable.

Figure 8 shows the progression of the first side lobe level for AUT #1. The blue curve represents the traditional acquisition case and appears to have converged after about 70% of the full data set has been acquired. The red curve again shows the rectangular spiral case and convergence is achieved after about 35% of the traditional data set. The green curve shows the adaptive rectangular

case with the array initialization and also converges after about 35% of the full data set. In this instance the adaptive acquisition techniques display a potential 80% reduction of test time for directivity and about 60% for the first side lobe.

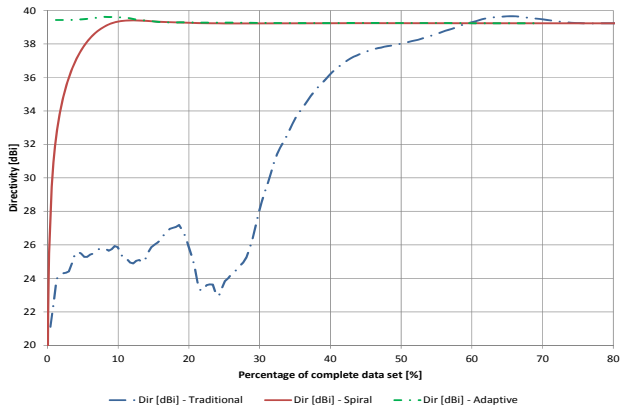

Figure 7 – Directivity value as a function of % acquisition for AUT #1. Traditional (blue), spiral (red) and rectangular loop adaptive (green).

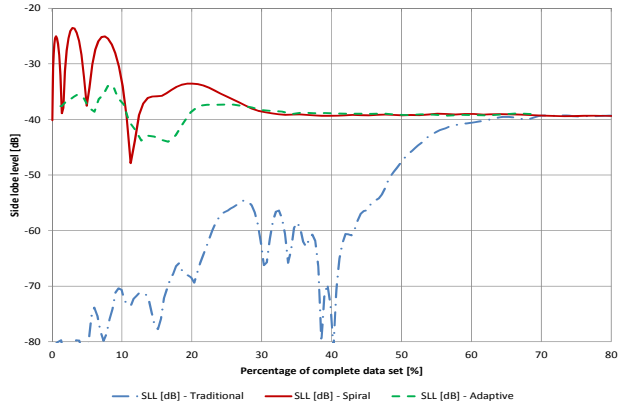

Figure 8 – First side lobe level as a function of % acquisition for AUT #1. Traditional (blue), spiral (red) and rectangular loop adaptive (green).

Figure 9 shows the progression of AUT directivity for AUT #2 as a function of relative acquisition time for the three acquisition methods. The blue curve again represents the traditional acquisition case and clearly shows little convergence during the initial acquisition phase. Final convergence is achieved at roughly 75% of the full data set. The red curve shows the rectangular spiral case and the rapid convergence is clear with a stable solution achieved at about 40%. The green curve shows the adaptive rectangular case with the array initialization applied and a stable directivity solution is achieved at about 5% of the full set acquisition time.

Data showing the progression of AUT directivity for AUT #3 as a function of acquisition time is similar to that presented above. Final convergence for the traditional acquisition is achieved at roughly 65% of the full data set and convergence for the spiral scanning is achieved at 30% while for the adaptive rectangular case with the array initialization applied, at about 15% of the traditional data set.

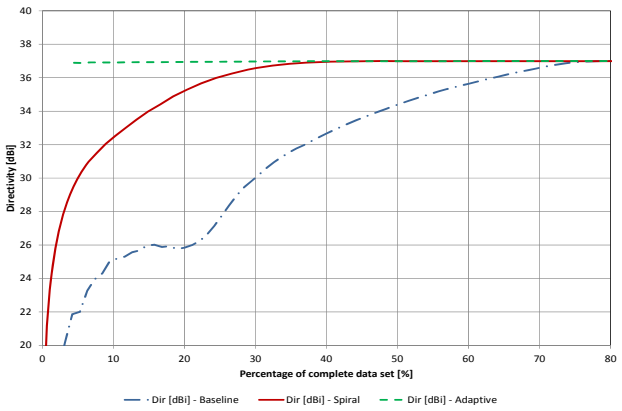

Figure 9 – Directivity value as a function of % acquisition for AUT #2. Traditional (blue), spiral (red) and rectangular loop adaptive (green).

AUT#4 is a monopulse antenna with difference pattern and was selected as test case to consider the impact of an irregular pattern on the adaptive techniques. Figure 10 below shows the progression of the difference pattern lobe maximum as a function of acquisition time for the three methods. The blue curve again represents the traditional acquisition case and clearly shows little convergence during the initial acquisition phase. Final convergence is achieved at roughly 65% of the full data set. The red curve shows the rectangular spiral case and the green the adaptive rectangular case with the array initialization applied. Both display convergence within about 20% of the traditional data set.

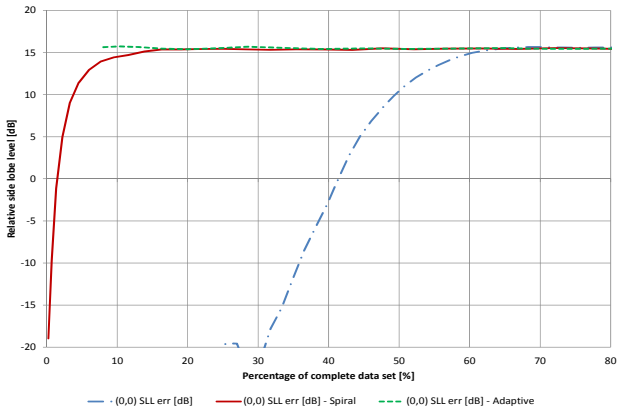

Figure 10 – Difference pattern lobe peak as a function of % acquisition for the monopulse antenna (AUT #4). Traditional (blue), rectangular spiral (red) and rectangular loop adaptive with array initialization (green).

Table 2 contains a summary of the four test cases considered for assessing test time reduction using the two adaptive techniques when considering pattern directivity (and difference pattern lobe maximum for AUT#4). Test time reductions are with respect to the complete acquired data set and not with respect to the convergence point of the traditional acquisition method.

Table 2 – Summary of test time reductions for AUT test cases considered.

AUT#	Antenna Type	Freq [GHz]	Potential test time reduction
1	Dual offset reflector	14.5 GHz	80%
2	Slotted waveguide array	23 GHz	60% - 90%
3	Offset reflector	12 GHz	70% - 85%
4	Monopulse antenna	10.5 GHz	80%

5 Measurement Results

Both the spiral acquisition and rectangular adaptive acquisition methods were implemented in hardware in order to obtain real test time estimates. Figure 11 below shows a comparison of the simulated test times versus the actual measured test times for both the traditional and the spiral scanning methods.

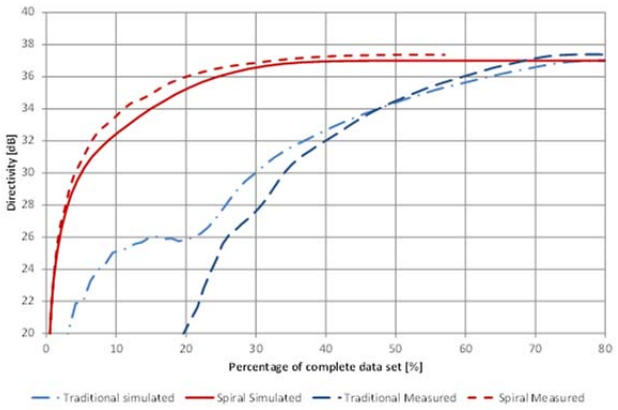

Figure 11 – Directivity value as a function of % acquisition for AUT #2. Simulation results versus actual measured test times are shown for the traditional (blue) and spiral (red) acquisition cases.

In this instance AUT #2 was used as test case and no near-field array initialization was performed. The data shows good agreement and validate simulated test times.

6 Conclusions

The results presented here represent further development of the methods previously proposed in [1 & 2]. There are three fundamental concepts presented:

1) The use of decision functions during a PNF acquisition process that allow for the reduction of test times by proceeding with data acquisition only until the quantities being sought are within the accuracy required.

2) Adaptive acquisition techniques that use the measured near-field data for guiding the regions of continued acquisition.

3) The use of near-field array initialization data based on two orthogonal measured near-field cuts.

These three concepts introduce computational aspects into the data acquisition stage in an effort to make acquisition processes more intelligent and ultimately reduce test times. The speed at which the far-zone field can be computed, makes this feasible.

Concept #1 above can easily be adopted for traditional acquisition methods currently in use and results presented here show that test time reductions of 20% - 40% may be possible by terminating acquisition based on an active far-field decision function.

Concept #2 above, represent a departure from the traditional PNF acquisition process. These methods have been implemented in rudimentary form and results are shown in Section 5. This data supports the simulation conclusions, showing that expected test time reductions are realistic and warrants further development of these adaptive techniques.

Concept #3 above can be used in conjunction with traditional acquisition methods or with adaptive techniques. The numerical data presented here shows that test time reductions of 60 % to 90% (depending on the parameter of interest) is possible by using this type of near-field array initialization. The overhead that this initialization requires is about 2% - 3% of the test time, which seems like a worthwhile penalty to concede for the convergence benefit to be gained.

The author would like to thank Mr Vincent Beaulé for the implementation of the adaptive near-field measurement routines and Prof Derek McNamara at the Univ of Ottawa for use of the test instrumentation.

7 References

[1] D.J. Janse van Rensburg, D. A. McNamara & G. Parsons, "Adaptive acquisition techniques for planar near-field antenna measurements", AMTA 33rd Annual Symposium, Denver, CO, USA, Oct. 2011.

[2] G. Parsons, D. A. McNamara & D.J. Janse van Rensburg, "An investigation of adaptive acquisition techniques for planar near-field antenna measurements", IEEE Antennas and Propagation Symposium Digest, Honolulu, HI, USA, June 2007.

[3] S. Gregson, J. McCormick & C. Parini, *Principles of Planar Near-Field Antenna Measurements* (IET Electromagnetic Wave Series, 2007).